

Learning an Object-Based Memory System

Yilun Du
MIT CSAIL

Joshua Tenenbaum
MIT CSAIL

Tomas Lozano-Perez
MIT CSAIL

Leslie Kaelbling
MIT CSAIL

Abstract—A robot operating in a household makes observations of multiple objects as it moves around over the course of days or weeks. The objects may be moved by inhabitants, but not completely at random. The robot may be called upon later to retrieve objects and will need a long-term object-based memory in order to know how to find them. In this paper, we combine some aspects of classic techniques for data-association filtering with modern attention-based neural networks to construct object-based memory systems that consume and produce high-dimensional observations and hypotheses. We perform end-to-end learning on labeled observation trajectories to learn both necessary internal transition and observation models. We demonstrate the system’s effectiveness on a sequence of problem classes of increasing difficulty and show that it outperforms clustering-based methods, classic filters, and unstructured neural approaches.

I. INTRODUCTION

Consider a robot operating in a household, making observations of multiple objects as it moves around over the course of days or weeks. The objects may be moved by the inhabitants, even when the robot is not observing them, and we expect the robot to be able to find any of the objects when requested. We will call this type of problem *entity monitoring*. It occurs in many applications, but we are particularly motivated by the robotics applications where the observations are very high dimensional, such as images or point clouds. Such systems need to perform online *data association*, determining which individual objects generated each observation, and *state estimation*, aggregating the observations of each individual object to obtain a representation that is lower variance and more complete than any individual observation. This problem can be addressed by an online recursive *filtering* algorithm that receives a stream of object detections as input and generates, after each input observation, a set of hypotheses corresponding to the actual objects observed by the agent.

When observations are closely spaced in time, the entity monitoring problem becomes one of *tracking* and it can be constrained by knowledge of the object dynamics. In many important domains, such as the household domain, temporally dense observations are not available, and so it is important to have systems that do not depend on continuous visual tracking.

A classical solution to the entity monitoring problem, developed for the tracking case but extensible to other dynamic settings, is a *data association filter* (DAF) (the tutorial of [2] provides a good introduction). A Bayes-optimal solution to this problem can be formulated, but it requires representing a number of possible hypotheses that grows exponentially with the number of observations. A much more practical, though less robust, approach is a maximum likelihood DAF (ML-OBM),

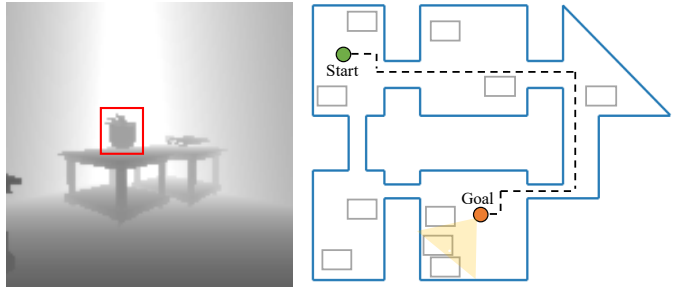


Fig. 1: (left) Example input observation to the OBM system. At each time-step, the OBM obtains a segmented depth map of a single object. (right) Example domain layout with a sample robot trajectory, field of view (in yellow) and tables that can contain objects. Objects in the domain can move both locally on the table they are currently resting on as well as to different tables (simulating perturbations induced by other household members.) The robot moves through the environment, getting local, partial observations of objects and must predict the number, location, and shape of objects it has seen throughout its trajectory.

which commits, on each step, to a maximum likelihood data association: the algorithm maintains a set of object hypotheses, one for each object (generally starting with the empty set) and for each observation it decides to either: (a) associate the observation with an existing object hypothesis and perform a Bayesian update on that hypothesis with the new data, (b) start a new object hypothesis based on this observation, or (c) discard the observation as noise. As the number of entities in the domain and the time between observations of the same entity increase, the problem becomes more difficult and begins to play the role of the long-term object-based memory (OBM) for an autonomous system with long time-horizons for memory and behavior.

The engineering approach to constructing a ML-OBM or OBM requires many design choices, including the specification of a latent state space for object hypotheses, a generative model relating observations to objects, and thresholds or other decision rules for choosing, for a new observation, whether to associate it with an existing hypothesis, use it to start a new hypothesis, or discard it. In any particular application, the engineer must tune all of these models and parameters to build an OBM that performs well. This is a time-consuming process that must be repeated for each new application.

A special case of entity monitoring is one in which the objects’ state is static, and does not change over time. In this case, a classical solution is online (robust) clustering. Clustering algorithms perform data association (cluster assignment) and

state estimation (computing a cluster “center”).

In this paper, we explore training neural networks to perform as OBM for dynamic entity monitoring and as online clustering methods for static entity monitoring. Although it is possible to train an unstructured RNN to solve these problems, we believe that building in some aspects of the structure of the OBM will allow faster learning with less data and allow the system to address problems with a longer horizon. We begin by briefly surveying the related literature, particularly focused on learning-based approaches. We then describe a neural-network architecture that uses self-attention as a mechanism for data association, and demonstrate its effectiveness in several illustrative problems. We find that it outperforms a raw RNN as well as domain-agnostic online clustering algorithms, and competitively with batch clustering strategies that can see all available data at once and with state-of-the-art systems for tracking with hand-built dynamics and observation models. Finally, we illustrate its application to problems with images as observations and long inter-observation gaps, in which both data association and the use of an appropriate latent space are critical.

II. RELATED WORK

Online clustering methods The typical setting for clustering problems is *batch*, where all the data is presented to the algorithm at once, and it computes either an assignment of data points to clusters or a set of cluster means, centers, or distributions. We are interested in the *online* setting, with observations arriving sequentially and a cumulative set of hypotheses output after each observation. One of the most basic online clustering methods is *vector quantization*, articulated originally by Gray [12] and understood as a stochastic gradient method by [16]. It initializes cluster centers at random and assigns each new observation to the closest cluster center, and updates that center to be closer to the observation. Methods with stronger theoretical guarantees, and those that handle unknown numbers of clusters have also been developed. Charikar et al. [7] formulate the problem of online clustering, and present several algorithms with provable properties. Liberty et al. [21] explore online clustering in terms of the facility allocation problem, using a probabilistic threshold to allocate new clusters in data. Choromanska and Monteleoni [9] formulate online clustering as a mixture of separate expert clustering algorithms.

Semantic mapping There is a large literature in robotics on *semantic mapping* and *semantic SLAM* (Kostavelis and Gasteratos [17] provide a good survey). Most of this work is focused on the spatial aspects of mapping, combined with semantic labeling of places and objects. The objects are generally static and long-term data-association is not emphasized; in addition the object types are known in advance and recognition models are hand-built or pre-trained. In our robotics experiments, we assume a fundamental capacity for SLAM and focus on constructing a memory of the objects in the environment, without prior models of the robot’s sensing, the types of objects to be encountered, or the patterns in which they might move in the environment.

Dynamic domains In the setting when the underlying entities have dynamics, such as airplanes observed via radar, a large number of DAFs have been developed. The most basic filter, for the case of a single entity and no data association problem, is the Kalman filter [33]. In the presence of data-association uncertainty the Kalman filter can be extended by considering assignments of observations to multiple existing hypotheses under the multiple hypothesis tracking (MHT) filter. A more practical approach that does not suffer from the combinatorial explosion of the MHT is the joint probabilistic data association (JPDA) filter, which keeps only one hypothesis but explicitly reasons about the most likely assignment of observations to hypotheses. [2] provides a detailed overview and comparison of these approaches, all of which require hand-tuned transition and observation models.

Learning for clustering There is a great deal of work using deep-learning methods to find latent spaces for clustering complex objects, particularly images. Min et al. [27] provide an excellent survey, including methods with auto-encoders, GANs, and VAEs. Relevant to our approach are *amortized inference* methods, including *set transformers* [19] and its specialization to *deep amortized clustering* [20], in which a neural network is trained to map directly from data to be clustered into cluster assignments or centers. A related method is *neural clustering processes* [28], which includes an online version, and focuses on generating samples from a distribution on cluster assignments, including an unknown number of clusters.

Visual data-association methods Data association has been explored in the context of visual object tracking [23, 35, 4, 5, 24, 31, 11]. In these problems, there is typically a fixed visual field populated with many smoothly moving objects. This is an important special case of the general data-association. It enables some specialized techniques that take advantage of the fact that the observations of each object are typically smoothly varying in space-time, and incorporate additional visual appearance cues. In contrast, in our setting, there is no fixed spatial field for observations and they may be temporally widely spaced, as would be the case when a robot moves through the rooms of a house, encountering and re-encountering different objects as it does so. Our emphasis is on this long-term data-association and estimation, and our methods are not competitive with specialized techniques on fixed-visual-field tracking problems.

Learning for data association There is relatively little work in the area of generalized data association, but Liu et al. [22] provide a recent application of LSTMs [13] to a rich version of the data association problem, in which batches of observations arrive simultaneously, with a constraint that each observation can be assigned to at most one object hypothesis. The sequential structure of the LSTM is used here not for recursive filtering, but to handle the variable numbers of observations and hypotheses. It is assumed that Euclidean distance is an appropriate metric and that the observation and state spaces are the same. Milan et al. [26] combine a similar use of LSTM for data association with a recurrent network that

learns to track multiple targets. It learns a dynamics model for the targets, including birth and death processes, but operates in simple state and observation spaces.

Algorithmic priors for neural networks One final comparison is to other methods that integrate algorithmic structure with end-to-end neural network training. This approach has been applied to sequential decision making by Tamar et al. [32], particle filters by [14], and Kalman filters by [18], as well as to a complex multi-module robot control system by [15]. The results generally are much more robust than completely hand-built models and much more sample-efficient than completely unstructured deep-learning. We view our work as an instance of this general approach.

III. PROBLEM FORMULATION

The problem of learning to perform online data association requires careful formulation. When the OBM is executed online, it will receive a stream of input observations z_1, \dots, z_T where $z_t \in \mathbb{R}^{d_z}$, and after each input z_t , it will output two vectors, $y_t = [y_{tk}]_{k \in (1..K)}$ and $c_t = [c_{tk}]_{k \in (1..K)}$, where $y_{tk} \in \mathbb{R}^{d_y}$, $c_{tk} \in (0, 1)$ and $\sum_k c_{tk} = 1$. The y values in the output represent the predicted properties of the hypothesized objects and the c values represent a measure of confidence in the hypotheses, in terms of the proportion of data that each one has accounted for. The maximum number of hypothesis “slots” is limited in advance to K . In some applications, the z and y values will be in the same space with the same representation, but this is not necessary.

We have training data representing N different data-association problems, $\mathcal{D} = \{(z_t^{(i)}, m_t^{(i)})_{t \in (1..L_i)}\}_{i \in (1..N)}$, where each training example is an input/output sequence of length L_i , each element of which consists of a pair of input z and $m = \{m_j\}_{j \in (1..J_t^{(i)})}$ which is a set of nominal object hypotheses representing the true *current state* of objects that have actually been observed so far in the sequence. It will always be true that $m_t^{(i)} \subseteq m_{t+1}^{(i)}$ and $J_t^{(i)} \leq K$.

Our objective is to train a recurrent computational model to perform as an OBM effectively in problems that are drawn from the same distribution as those in the training set. To do so, we formulate a model (described in section IV) with parameters θ , which transduces the input sequence z_1, \dots, z_L into an output sequence $(y_1, c_1), \dots, (y_L, c_L)$, and train it to minimize the following loss function:

$$\mathcal{L}(\theta; \mathcal{D}) = \sum_{i=1}^N \sum_{t=1}^{L_i} \mathcal{L}_{\text{obj}}(y_t^{(i)}, m_t^{(i)}) + \mathcal{L}_{\text{slot}}(y_t^{(i)}, c_t^{(i)}, m_t^{(i)}) + \mathcal{L}_{\text{sparse}}(c_t^{(i)}) .$$

The \mathcal{L}_{obj} term is a *chamfer loss* [3], which looks for the predicted y that is closest to each actual m_k and sums their distances, making sure the model has found a good, high-confidence representation for each true object:

$$\mathcal{L}_{\text{obj}}(y, m) = \sum_j \min_k \frac{1}{c_k + \epsilon} \|y_k - m_j\| .$$

The $\mathcal{L}_{\text{slot}}$ term is similar, but makes sure that each object the model has found is a true object, where we multiply by c_k to not penalize for predicted objects in which we have low confidence:

$$\mathcal{L}_{\text{slot}}(y, c, m) = \sum_k \min_j c_k \|y_k - m_j\| .$$

The sparsity loss discourages the model from using multiple outputs to represent the same true object:

$$\mathcal{L}_{\text{sparse}}(c) = -\log \|c\| .$$

IV. OBM-NETS

Inspired by the the basic form of classic DAF algorithms and the ability of modern neural-network techniques to learn complex models, we have designed the OBM-Net architecture for learning DAFs and a customized procedure for training it from data, inspired by several design considerations. First, because object hypotheses must be available after each individual input and because observations will generally be too large and the problem too difficult to solve from scratch each time, the network will have the structure of a recursive filter, with new memory values computed on each observation and then fed back for the next. Second, because the loss function is *set based*, that is, it doesn’t matter what order the object hypotheses are delivered in, our memory structure should also be permutation invariant, and so the memory processing is in the style of an attention mechanism. Finally, because in some applications the observations z may be in a representation not well suited for hypotheses representation and aggregation, the memory operates on a latent representation that is related to observations and hypotheses via encoder and decoder modules.

Figure 2 shows the architecture of the OBM-Net model. There are six modules with adaptable weights and memory that is stored in two recurrent quantities, s and n . The main memory is s , which consists of K elements, each in \mathbb{R}^{d_s} ; the length- K vector n of positive values encodes how many observations so far have been assigned to each slot. When an input z arrives, it is immediately *encoded* into a vector e in \mathbb{R}^{d_s} . The *update* network operates on the encoded input and the contents of each hypothesis slot, intuitively producing an update of the hypothesis in that slot under the assumption that the current z is an observation of the object represented by that slot; so for all slots k ,

$$u_k = \text{update}(s_k, n_k, e) .$$

The *attention* weights w represent the degree to which the current input “matches” the current value:

$$w_k = \frac{\exp(\text{attend}(s_k, n_k, e))}{\sum_{j=0}^n \exp(\text{attend}(s_j, n_k, e))} .$$

To force the network to commit to a sparse assignment of observations to object hypotheses while retaining the ability to effectively train with gradient descent, the *suppress* module sets all but the top M values in w to 0 and renormalizes, to obtain the vector a of M values that sum to 1. The a vectors

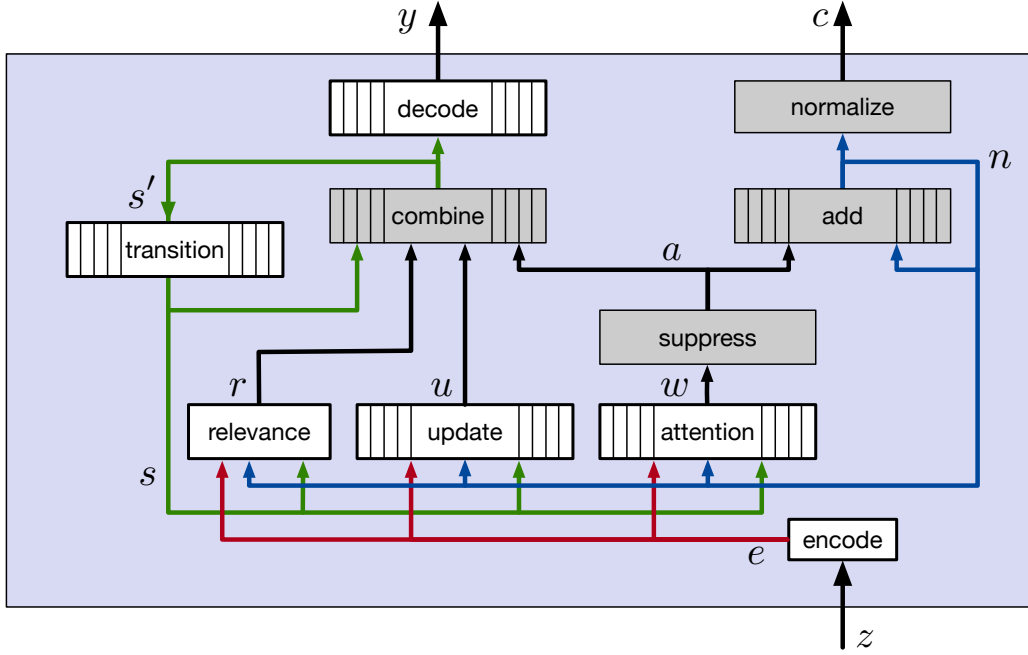


Fig. 2: Architecture of the OBM-Net. Grey boxes represent fixed computations; white boxes represent neural networks with adjustable parameters; those with internal vertical bars represent a replication of the same computation on slot values in parallel. Red lines indicate information derived from an input observation, green lines indicate information derived from hypothesis slot values, and blue lines indicate information derived from counts on each hypothesis slot.

are integrated to obtain n , which is normalized to obtain the final output confidence values c .

Additionally, a scalar *relevance* value, $r \in (0, 1)$, is computed from s and e ; this value is used to modulate the degree to which slot values are updated, and gives the machine the ability to ignore or downweight an input. It is computed as

$$r = \text{NN}_1(\text{avg} \sum_{k=1}^K \text{NN}_2(e, s_k, n_k)) ,$$

where NN_1 is a fully connected network with the same input and output dimensions and NN_2 is a fully connected network with a sigmoid output unit. The attention output a and relevance r are now used to decide how to combine all possible slot-updates u with the old slot values s_t using the following fixed formula for each slot k :

$$s'_{tk} = (1 - r a_k) s_{tk} + r a_k u_k .$$

Because most of the a_k values have been set to 0, this results in a sparse update which will ideally concentrate on a single slot to which this observation is being “assigned.”

To compute the outputs, the s'_t slot values are decoded into the representation that is required for the outputs, y :

$$y_k = \text{decode}(s'_{tk}) .$$

Finally, to handle the setting in which object state evolves over time, we can further add a dynamics model, which computes the state s_{t+1} from the new slot values s'_t using an additional neural network:

$$s_{t+1k} = \text{NN}_3(s'_{tk}) .$$

These values are fed back, recurrently, as inputs to the overall

system.

Given a data set \mathcal{D} , we train the OBM-Net model end-to-end to minimize loss function \mathcal{L} , with a slight modification. We find that including the $\mathcal{L}_{\text{sparse}}$ term from the beginning of training results in poor learning, but adopting a training scheme in which the $\mathcal{L}_{\text{sparse}}$ is first omitted then reintroduced over training epochs, results in reliable training that is efficient in both time and data.

V. EMPIRICAL RESULTS

We evaluate OBM-Net on several *entity monitoring* tasks, including simple online clustering, monitoring objects with dynamics, and high-dimensional image pose prediction in which the observation space is not the same as the hypothesis space. We then combine all of these challenges in the simulated household robot domain shown in Figure 1. Our experiments aim to substantiate the following claims:

- OBM-Net outperforms non-learning clustering methods, even those that operate in batch mode rather than online, because those methods cannot learn from experience to take advantage of information about the distribution of observations and true object properties (tables II, I, VI and VIII).
- OBM-Net outperforms clustering methods that can learn from previous example problems when data is limited, because it provides useful structural bias for learning (table II, I and VI).
- OBM-Net generalizes to differences between training and testing in (a) the numbers of actual objects, (b) the numbers of hypothesis slots and (c) the number of observations (tables II and III).

Model	Online	Learned	Normal	Elongated	Mixed	Angular	Noise
OBM-Net	+	+	0.157 (0.001)	0.191 (0.001)	0.184 (0.001)	0.794 (0.001)	0.343 (0.001)
Set Transformer	+	+	0.407 (0.001)	0.395 (0.001)	0.384 (0.001)	0.794 (0.003)	0.424 (0.001)
LSTM	+	+	0.256 (0.001)	0.272 (0.001)	0.274 (0.001)	0.799 (0.002)	0.408 (0.001)
VQ	+	-	0.173 (0.002)	0.195 (0.002)	0.191 (0.002)	0.992 (0.004)	0.947 (0.002)
Set Transformer	-	+	0.226 (0.001)	0.248 (0.001)	0.274 (0.001)	0.816 (0.001)	0.406 (0.002)
K-means++	-	-	0.103 (0.001)	0.139 (0.001)	0.135 (0.001)	0.822 (0.003)	1.259 (0.002)
GMM	-	-	0.113 (0.001)	0.141 (0.001)	0.136 (0.001)	0.865 (0.003)	1.207 (0.002)

TABLE I: Comparison of performance on clustering after 30 iterations when training on 1000 different distributions for a thousand iterations. We use a total of 3 components, and train models with 30 observations. We report standard error in parentheses. Each cluster observation and center is drawn between -1 and 1, except for angular which is drawn between $-\pi$ and π with reported error as the L2 distance between predicted and ground truth mean with standard error in parentheses.

- OBM-Net is able to learn dynamics models and observation functions for the setting when the entities are moving over time (table V and VIII), nearly matching the performance of strong data association filters with known ground-truth models.
- OBM-Net works when significant encoding and decoding are required (table, VI, VII and VIII), .
- OBM-Net can learn to work effectively in domains that combine high-dimensional inputs and outputs with object dynamics and long between-observation time lapses (tables VIII and IX).

We compare with the following alternative methods: **Batch, non-learning**: K-means++ [1] and expectation maximization (EM) [10] on a Gaussian mixture model (SciKit Learn implementation); **Online, non-learning**: vector quantization [12]; **Batch, learning**: set transformer [19]; **Online, learning**: LSTM [13] and an online variant of the set transformer [19]; **Dynamic, non-learning**: joint probabilistic data association filter [2]. All learned network architectures are set to have about 50000 parameters. We provide additional details about architecture and training in the appendix. The set transformer is a standard architecture that has been evaluated on clustering problems in the past.

All models except OBM-Net are given the ground truth number of components K , while OBM-Net uses 10 hypothesis slots. Results are reported in terms of loss $\sum_j \min_k \|y_k - m_j\|$ (with the most confident K hypotheses selected for OBM-Net).

A. Gaussian domains

To check the basic operation of the model and understand the types of problems for which it performs well, we tested in simple clustering problems with the same input and output spaces, but different types of data distributions, each a mixture of three components. We train on 1000 problems drawn from each problem distribution distribution and test on 5000 from the same distribution. In every case, the means of the three components are drawn at random for each problem.

- 1) *Normal*: Each component is a 2D Gaussian with fixed identical variance across each individual dimension and across distributions. This is a basic “sanity check.”
- 2) *Elongated*: Each component is a 2D Gaussian, where the variance along each dimension is drawn from a uniform distribution, but fixed across distributions.
- 3) *Mixed*: Each component is a 2D Gaussian, with fixed identical variance across each individual dimension, but

Model	Online	Learned	Observations				
			10	30	50	100	
OBM-Net	+	+	0.235 (0.001)	0.162 (0.001)	0.146 (0.001)	0.121 (0.001)	
Set Transformer	+	+	0.390 (0.002)	0.388 (0.002)	0.388 (0.002)	0.389 (0.001)	
LSTM	+	+	0.288 (0.001)	0.260 (0.001)	0.269 (0.001)	0.288 (0.001)	
VQ	+	-	0.246 (0.001)	0.172 (0.001)	0.147 (0.001)	0.122 (0.001)	
Set Transformer	-	+	0.295 (0.003)	0.261 (0.001)	0.253 (0.001)	0.247 (0.001)	
K-means++	-	-	0.183 (0.002)	0.107 (0.001)	0.086 (0.001)	0.066 (0.001)	
GMM	-	-	0.189 (0.002)	0.118 (0.001)	0.087 (0.001)	0.067 (0.001)	

TABLE II: Comparison of performance after training on one thousand *Normal* distributions for a thousand iterations. We use 3 components, and train models with 30 observations. We report standard error in parentheses. Each cluster observation and center is drawn between -1 and 1, with reported error as the L2 distance between predicted and ground truth mean.

with the variance of each distribution drawn from a uniform distribution.

- 4) *Angular*: Each component is a 2D Gaussian with identical variance across dimension and distribution, but points above π are wrapped around to $-\pi$ and points below $-\pi$ wrapped to π
- 5) *Noise*: Each component has 2 dimensions parameterized by Gaussian distributions, but with the values of the remaining 30 dimensions drawn from a uniform distribution centered at 0.

We compare our approach to each of the non-dynamic baselines for the five problem distributions in Table II; a complete listing of results for all the distributions can be found in the Appendix. The results in this table show that on *Normal*, *Mixed*, and *Elongated* tasks, OBM-Net performs comparably to the offline clustering algorithms, even though it is running and being evaluated online. On the *Angular* and *Noise* tasks, OBM-Net is able to learn a useful metric for clustering and outperforms both offline and online alternatives (with additional analysis in the appendix showing OBM-Net outperforms all other learning baselines with more training distributions in the *Angular* task).

In Table II we evaluate the quality of predictions after 10, 30, 50, and 100 observations in the *Normal* distribution. We find that OBM-Net generalizes well to increased numbers of observations, with predictions becoming more accurate as the observation sequence length increases, despite the fact that it is trained only on observation sequences of length 30. This is in contrast with other online learning baselines, set transformer and LSTM, which both see increases in error after 50 or 100 observations. This pattern holds across all the test problem distributions (see Appendix).

In Table III, we investigate the generalization ability of

Model	Slots	Ground Truth Clusters		
		3	5	7
OBM-Net	10	0.162 (0.001)	0.214 (0.001)	0.242 (0.001)
	20	0.175 (0.001)	0.195 (0.001)	0.213 (0.001)
	30	0.188 (0.001)	0.197 (0.001)	0.205 (0.001)
Set Transformer	-	0.261 (0.001)	0.279 (0.001)	0.282 (0.001)
Vector Quantization	-	0.171 (0.001)	0.199 (0.001)	0.205 (0.001)

TABLE III: Quantitative evaluation of OBM-Net on distributions with different numbers of true components and hypothesis slots *at test time* with 30 observations. In all cases, OBM-Net is trained with 3-component problems, 10 slots, and 30 observations. We compare with an offline set transformer trained with different numbers of problem components as well as with vector quantization.

Sparsity	Learned Memory	Supression	Relevance	Observations			
				10	30	50	100
-	-	-	-	0.382 (0.003)	0.452 (0.003)	0.474 (0.003)	0.487 (0.003)
+	-	-	-	0.384 (0.001)	0.412 (0.001)	0.423 (0.001)	0.430 (0.003)
+	+	-	-	0.335 (0.002)	0.357 (0.002)	0.366 (0.003)	0.387 (0.001)
+	+	+	-	0.279 (0.001)	0.274 (0.001)	0.278 (0.001)	0.282 (0.001)
+	+	+	+	0.238 (0.001)	0.157 (0.001)	0.137 (0.001)	0.131 (0.001)

TABLE IV: We ablate each component of OBM-Net on the *Normal* distribution. When learned memory is ablated, OBM-Net updates states based on observed values (appropriate in the Normal Distribution dataset).

OBM-Net to both increases in the number of hypothesis slots and the underlying number of mixture components from which observations are drawn. We compare to the offline set transformer and to VQ, both of which know the correct number of components at test time. Recall that, to evaluate OBM-Net even when it has a large number of extra slots, we use its K most confident hypotheses. We find that OBM-Net generalizes well to increases in hypothesis slots, and exhibits improved performance with large number of underlying components, performing comparably to or better than the VQ algorithm. We note that none of the *learning* baselines can adapt to different numbers cluster components at test time, but find that OBM-Net outperforms the set transformer even when it is trained on the ground truth number of clusters in the test.

We also ablate each component of our model and the results are shown in Table IV; we found that each of our proposed components enables both better performance and generalization. Additional analysis and illustrations of the clustering process are in the appendix.

B. Dynamic Domains

We next evaluate the ability of OBM-Net to perform data association in domains where objects are moving dynamically over time. This domain is typical of tracking problems considered by data association filters, and we compare with the de-facto standard method, Joint Probabilistic Data Association (JPDA), which uses hand-built ground-truth models. We consider a setup consisting of 3 different moving objects in 2D. Their velocity is perturbed at each step by an additive component drawn from a Gaussian distribution and observations of their positions (but no observations of velocities) are made with Gaussian error. To perform well in this task, a model must discover that it needs to estimate the latent velocity of

Model	Observations			
	10	20	30	40
OBM-Net	0.415 (0.009)	0.395 (0.007)	0.382 (0.007)	0.394 (0.006)
Online Set Transformer	0.699 (0.009)	0.701 (0.010)	0.854 (0.017)	1.007 (0.018)
LSTM	0.422 (0.009)	0.400 (0.006)	0.445 (0.007)	0.464 (0.005)
JPDA (ground truth)	0.683 (0.030)	0.372 (0.034)	0.362 (0.034)	0.322 (0.034)

TABLE V: Comparison of performance on position estimation of 3 dynamically moving objects. All learning models are trained with 1000 sequences of 30 observations. We report MSE error with standard error in parentheses. JPDA uses the ground-truth observation and dynamics models.

each object, as well as learn the underlying dynamics and observation models.

We compare our approach to the Set Transformer and LSTM methods, as well as to JPDA with ground-truth models. The basic clustering methods have no ability to handle dynamic systems so we omit them from the comparison. The learning methods (OBM-Net, Set Transformer, and LSTM) are all trained on observation sequences of length 30. We test performance of all four methods on sequences of multiple lengths. Quantitative performance, measured in terms of prediction error on true object locations, is reported in Table V. We can see that the online Set Transformer cannot learn a reasonable model at all. The LSTM performs reasonably well for short (length 30) sequences but quickly degrades relative to OBM-Net and JPDA as sequence length increases. We note that OBM-Net performs comparably to but just slightly worse than JPDA. This is strong performance because OBM-Net is generic and can be adapted to new domains given training data without the need to hand-design the models used by JPDA.

C. Image-based domains

We further evaluate the ability of OBM-Net to perform data association in domains with substantially more complex observation spaces, where the outputs are not simple averages of the inputs. This requires the network to synthesize a latent representation for slots in which the simple additive update performs effectively.

We investigate this with two image-based domains. In each domain, we have a set of similar objects (digits or airplanes). A *problem* is constructed by selecting K objects from the domain, and the desired y values are images of those objects in a canonical viewpoint. The input observation sequence is generated by randomly selecting one of those K objects, and then generating an image of it from a random viewpoint as the observation z .

Our two domains are: (1) **MNIST**: Each object is a random image in MNIST, with observations corresponding to a rotated images, and the desired outputs being the un-rotated images; (2) **Airplane**: Each object is a random object from the Airplane class in ShapeNet [6], with observations corresponding to airplane renderings (using Blender) at different viewpoints and the desired outputs the objects rendered in a canonical viewpoint.

For MNIST, we use the 50000 images in the training set to construct the training problems, and the 10000 images in the non-overlapping test set to construct the test problems. For

Type	Model	Learned	Observations			
			10	30	50	100
MNIST	OBM-Net	+	7.143 (0.006)	5.593 (0.004)	5.504 (0.004)	5.580 (0.004)
	LSTM	+	9.980 (0.005)	9.208 (0.004)	9.166 (0.004)	9.267 (0.004)
	K-means (Pixel)	-	13.214 (0.005)	12.010 (0.005)	11.961 (0.004)	11.719 (0.004)
	K-means (Learned)	+	13.596 (0.006)	12.505 (0.005)	12.261 (0.003)	12.021 (0.004)
Airplanes	OBM-Net	+	4.558 (0.005)	4.337 (0.004)	4.331 (0.004)	4.325 (0.004)
	LSTM	+	5.106 (0.003)	4.992 (0.005)	4.983 (0.003)	4.998 (0.004)
	K-means (Pixel)	-	7.127 (0.006)	6.890 (0.004)	6.603 (0.004)	6.517 (0.004)
	K-means (Learned)	+	7.246 (0.006)	6.943 (0.005)	6.878 (0.005)	6.815 (0.004)

TABLE VI: Comparison of performance of online clustering on MNIST and on rendered Airplane dataset. For OBM-Net, LSTM and K-means (Learned) we use a convolutional encoder/decoder trained on the data; for K-means (Pixel) there is no encoding. We use a total of 3 components and train models with 30 observations. Models are trained on 20000 problems on both datasets.

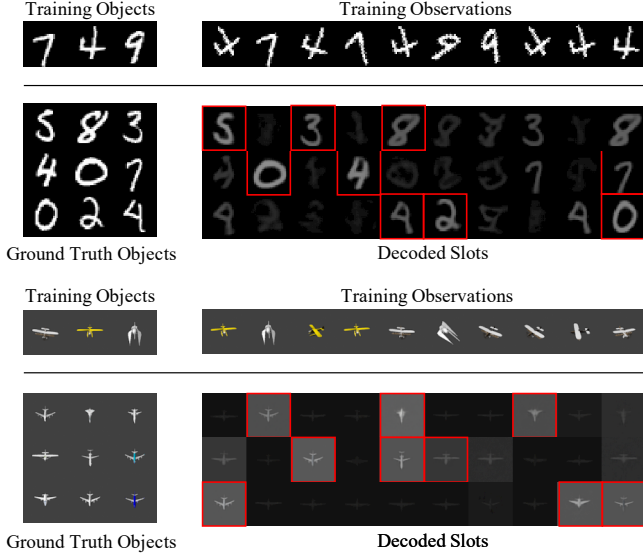


Fig. 3: Results on two image-based association tasks (left: MNIST, right: airplanes). At the top of each is an example training problem, illustrated by the true objects and an observation sequence. Each of the next rows shows an example test problem, with the ground truth objects and decoded slot values. The three highest-confidence hypotheses for each problem are highlighted in red, and correspond nicely to ground truth slots.

the Airplane dataset, we use 1895 airplanes to construct the training problems, and 211 different airplanes to construct the test problems. Each airplane is rendered with 300 viewpoints.

In this setting, of our baseline methods, only batch K-means (in pixel space) can be directly applied to this problem with even reasonable results. We also include versions of LSTM and of batch K-means that operate on a latent representation that is learned first using an auto-encoder. In Table VI, we find that our approach significantly outperforms other comparable baselines in both accuracy and generalization. We visualize qualitative predictions from our model in Figure 3. We find that our highest confidence decoded slots correspond nicely to ground truth slots – with less confident slots decoding to mean shape values.

In addition, we consider the setting when each of K objects are moving across time. We utilize our MNIST setup, but initialize digits at a random position in the image (with parts of a digit that are outside of the image wrapped around to the other side of the image). At each timestep, the center of

Model	Learned	Observations			
		10	30	50	100
OBM-Net	+	13.207 (0.003)	13.214 (0.004)	18.318 (0.006)	14.743 (0.003)
LSTM	+	15.076 (0.008)	15.132 (0.006)	19.134 (0.004)	16.071 (0.006)
K-means (Pixel)	-	18.378 (0.005)	18.817 (0.005)	20.269 (0.005)	18.407 (0.006)
K-means (Learned)	+	31.127 (0.003)	31.127 (0.003)	31.127 (0.003)	31.127 (0.003)

TABLE VII: Comparison of performance on regressing the ground truth un-rotated version of an MNIST digit where digits move over time. For OBM-Net, LSTM and K-means (Learned) we use a convolutional encoder/decoder trained on the data; for K-means (Pixel) there is no encoding. We use a total of 3 components and train models with 30 observations. We report MSE error with respect to ground truth unrotated images.

each moves with a constant velocity, with the goal to predict the un-rotated image at the current center of digit. We report results with baselines in Table VII and find that our approach performs well in this setting also.

D. Simulated Household Robot Domains

Finally, we show that by being able to do data association on complex observation spaces and dynamic objects, OBM-Net enables us to perform well on the complex long-term object state estimation tasks described in the introduction of the paper.

In this setting, we construct a house domain, consisting of five separate rooms as pictured in Figure 1 in the PyBullet simulation environment. We sample a total of 8 separate tables in the house, with each table supporting two objects, drawn from 3 classes, each with its own distinctive character of motion. A *problem* is then constructed by sampling a robot trajectory of length of 50 (corresponding to exploration of 4-5 rooms in the house); the desired output y values being, for each object seen so far, the predicted table y^t it was on as well its associated offsets relative to the predicted table, y^o . The input sequence of observations z corresponds to a segmented depth map of a single object visible given the camera pose at a particular timestep (or an empty observation in the case no object is visible – which occurs for roughly 70% of observed trajectory timesteps), as well as which table it is resting on and its positional offset relative to the table. Note that we are *not* solving the SLAM problem, and are assuming the existence of moderately accurate robot localization, which allows us to predict which particular table the robot is observing; the object point-clouds are observed relative to the table frame, which is a reliable local computation.

We train on a total of 20000 randomly sampled trajectories in the same floor plan, but with new randomly drawn object

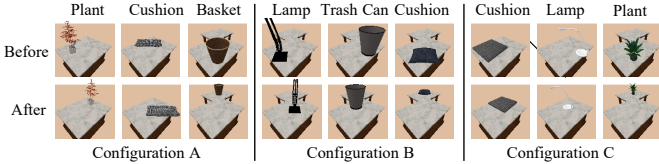


Fig. 4: Illustration of movement patterns of each class of objects in each configuration. Before and after images show 20 timesteps of motion. Each class contains around 10 differently-shaped objects.

Configuration	Model	Learned	Table Accuracy			Position Error		
Observations			10	25	50	10	25	50
A	OBM-Net	+	0.984	0.926	0.809	0.019	0.041	0.078
	LSTM	+	0.839	0.661	0.406	0.058	0.093	0.126
	K-means	-	0.761	0.695	0.485	0.053	0.070	0.103
B	OBM-Net	+	0.989	0.924	0.795	0.021	0.046	0.082
	LSTM	+	0.875	0.716	0.514	0.053	0.094	0.123
	K-means	-	0.761	0.695	0.488	0.053	0.070	0.103
C	OBM-Net	+	0.988	0.932	0.873	0.027	0.052	0.080
	LSTM	+	0.892	0.717	0.519	0.052	0.091	0.130
	K-means	-	0.761	0.695	0.488	0.053	0.069	0.103

TABLE VIII: Comparison of performance of our method on the realistic robotics configuration of different objects on three different world-dynamics configurations.

instances and tables for each trajectory. We test using 1000 trajectories, with test object meshes drawn from a set *disjoint from* the set of object meshes used during training (but sharing the same semantic class). To test the flexibility of the approach, we consider three separate configurations of object classes on tables, which we illustrate in Figure 4.

- Configuration A: Plants (which move horizontally across a table), cushions (which move vertically across a table), and baskets (which move diagonally in a table, but also teleport sequentially to different tables).
- Configuration B: Table Lamps (which move horizontally), Trash Cans (which move vertically) and cushions (which move diagonally across a table, but also sequentially teleport between tables).
- Configuration C: Cushions (which move horizontally), Table Lamps (which move vertically) and plants (which move diagonally across a table, but also sequentially teleport between tables).

To test the efficacy of our approach, we measure to what extent each hypothesis slot m_i can recover both the table that the associated object is on, as well as its position relative to the table. We match a hypothesis slot k with each object label y_i by computing $\arg \min_k \|y_i^o - m_k^o\| + \text{Loss}_{\text{CE}}(y_i^c - m_k^c)$. For each match, we report the accuracy of m_k^c matching y_i^c , and as well the mean absolute error between y_i^o and m_k^o . When the

Model	Learned	Steps Since Observation			
		10	20	30	40
OBM-Net	+	0.841	0.839	0.767	0.673
LSTM	+	0.593	0.508	0.437	0.367
K-means	-	0.577	0.572	0.573	0.573

TABLE IX: Performance of each method on regressing the table that each object is on compared to the number of steps since the last observation of the object.

table prediction for y_i is incorrect, we set mean absolute error to be equal to half the table size (0.15), as reported table offsets are meaningless in that case. Both OBM-Net and associated baselines use 10 hypothesis slots.

In this setting, we consider batch K-means as a baseline method to obtain a set of object hypotheses for our scene. For each input-segmented depth map, we obtain an estimate of the offset of the object from a table by averaging all coordinates in the segmented depth map. We then apply batch K-means clustering to all computed offsets and corresponding table ids. This baseline has more “built-in” understanding of the problem than OBM-Net. We further compare with an LSTM on a learned latent space. For both the LSTM baseline and OBM-Net, we project segmented depth maps to a 3D pointcloud and randomly sub-sample to obtain 100 points, utilizing a MLP to map both points and table identities to latent features.

We quantitatively compare OBM-Net with baselines in Table VIII. Our approach outperforms both baselines in both estimating the supporting tables and regressing the position of each individual object relative to its predicted table. Next, we analyze the error of our approach and baselines, as a function of the number of steps since we have seen an object in Table IX and observe that it is substantially better at long-term memory than the LSTM, and still outperforms K-means even with long inter-observation gaps. By adding a shape occupancy prediction head [25, 29, 8] to OBM-Net, we can also regress the underlying 3D shapes of our objects. We predict each shape at 32x32x32 resolution, decoding each occupancy at each voxel coordinate using a MLP head conditioned on a hypothesis state. We illustrate different reconstructions of shape compared to ground truth in Figure 5. We find that our approach is able to aggregate depth information to obtain the resultant 3D reconstructed shape. Quantitatively, we find that our approach gets 95.33% accuracy in regressing voxels for each test mesh in the test set.

VI. DISCUSSION

This work has demonstrated that using algorithmic bias inspired by a classical solution to the problem of filtering to estimate the state of multiple objects simultaneously, coupled with modern machine-learning techniques, we can arrive at solutions that learn to perform and generalize well. Importantly, the same underlying system, with *no prior knowledge* about the types of observations or desired output hypotheses or the frequency of observations, is able to learn to perform data-association and state estimation to solve a variety of clustering problems as well as to support an object-based memory system for a robot in a dynamically changing environment.

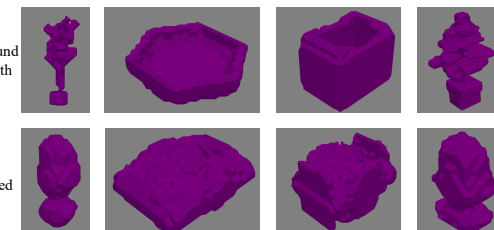


Fig. 5: Illustration of predicted 3D reconstructions on test meshes compared to ground truth meshes.

REFERENCES

[1] David Arthur and Sergei Vassilvitskii. k-means++: the advantages of careful seeding. In *Symposium on Discrete Algorithms '07*, 2007.

[2] Yaakov Bar-Shalom, Fred Daum, and Jim Huang. The probabilistic data association filter. *IEEE Control Systems Magazine*, December 2009.

[3] Harry G. Barrow, Jay M. Tenenbaum, Robert C. Bolles, and Helen C. Wolf. Parametric correspondence and chamfer matching: Two new techniques for image matching. In *IJCAI*, 1977.

[4] Alex Bewley, Zongyuan Ge, Lionel Ott, Fabio Ramos, and Ben Upcroft. Simple online and realtime tracking. In *2016 IEEE International Conference on Image Processing (ICIP)*, pages 3464–3468, 2016.

[5] Guillem Brasó and Laura Leal-Taixé. Learning a neural solver for multiple object tracking. In *The IEEE Conference on Computer Vision and Pattern Recognition (CVPR)*, June 2020.

[6] Angel X Chang, Thomas Funkhouser, Leonidas Guibas, Pat Hanrahan, Qixing Huang, Zimo Li, Silvio Savarese, Manolis Savva, Shuran Song, Hao Su, Jianxiong Xiao, Li Yi, and Fisher Yu. Shapenet: An information-rich 3d model repository. *ArXiv:1512.03012*, 2015.

[7] Moses Charikar, Chandra Chekuri, Tomás Feder, and Rajeev Motwani. Incremental clustering and dynamic information retrieval. *SIAM Journal on Computing*, 33(6):1417–1440, 2004.

[8] Zhiqin Chen and Hao Zhang. Learning implicit fields for generative shape modeling. In *Proceedings of the IEEE Conference on Computer Vision and Pattern Recognition*, pages 5939–5948, 2019.

[9] Anna Choromanska and Claire Monteleoni. Online clustering with experts. In *Artificial Intelligence and Statistics*, pages 227–235, 2012.

[10] Arthur P Dempster, Nan M Laird, and Donald B Rubin. Maximum likelihood from incomplete data via the em algorithm. *Journal of the Royal Statistical Society: Series B (Methodological)*, 39(1):1–22, 1977.

[11] Davi Frossard and Raquel Urtasun. End-to-end learning of multi-sensor 3d tracking by detection. In *ICRA*, May 2018.

[12] R. Gray. Vector quantization. *IEEE ASSP Magazine*, 1(2):4–29, 1984.

[13] Sepp Hochreiter and Jürgen Schmidhuber. Long short-term memory. *Neural Comput.*, 9(8):1735–1780, 1997.

[14] Rico Jonschkowski, Divyam Rastogi, and Oliver Brock. Differentiable particle filters: End-to-end learning with algorithmic priors. *ArXiv*, abs/1805.11122, 2018.

[15] Peter Karkus, Xiao Ma, David Hsu, Leslie Pack Kaelbling, Wee Sun Lee, and Tomas Lozano-Perez. Differentiable algorithm networks for composable robot learning. *ArXiv*, abs/1905.11602, 2019.

[16] Teuvo Kohonen. *Self-Organizing Maps*. Springer-Verlag, 1995.

[17] Ioannis Kostavelis and Antonios Gasteratos. Semantic mapping for mobile robotics tasks: A survey. *Robotics and Autonomous Systems*, 66:86–103, 2015.

[18] Rahul G. Krishnan, Uri Shalit, and David A Sontag. Deep kalman filters. *ArXiv*, abs/1511.05121, 2015.

[19] Juho Lee, Yoonho Lee, Jungtaek Kim, Adam R Kosiorek, Seungjin Choi, and Yee Whye Teh. Set transformer: A framework for attention-based permutation-invariant neural networks. *arXiv preprint arXiv:1810.00825*, 2018.

[20] Juho Lee, Yoonho Lee, and Yee Whye Teh. Deep amortized clustering. *ArXiv*, abs/1909.13433, 2019.

[21] Edo Liberty, Ram Sriharsha, and Maxim Sviridenko. An algorithm for online k-means clustering. In *2016 Proceedings of the eighteenth workshop on algorithm engineering and experiments (ALENEX)*, pages 81–89. SIAM, 2016.

[22] Huajun Liu, Hui Zhang, and Christoph Mertz. DeepDA: LSTM-based deep data association network for multi-targets tracking in clutter. In *2019 22th International Conference on Information Fusion (FUSION)*, pages 1–8, 2019.

[23] Wenhao Luo, Junliang Xing, Anton Milan, Xiaoqin Zhang, Wei Liu, Xiaowei Zhao, and Tae-Kyun Kim. Multiple object tracking: A literature review. *arXiv preprint arXiv:1409.7618*, 2014.

[24] Cong Ma, Yuan Li, Fan Yang, Ziwei Zhang, Yueqing Zhuang, Huizhu Jia, and Xiaodong Xie. Deep association: End-to-end graph-based learning for multiple object tracking with conv-graph neural network. In *International Conference on Multimedia Retrieval (ICMR)*, June 2019.

[25] Lars Mescheder, Michael Oechsle, Michael Niemeyer, Sebastian Nowozin, and Andreas Geiger. Occupancy networks: Learning 3d reconstruction in function space. In *Proceedings of the IEEE Conference on Computer Vision and Pattern Recognition*, pages 4460–4470, 2019.

[26] Anton Milan, Seyed Hamid Rezatofighi, Anthony R. Dick, Ian Reid, and Konrad Schindler. Online multi-target tracking using recurrent neural networks. *ArXiv*, abs/1604.03635, 2017.

[27] Erxue Min, Xifeng Guo, Qiang Liu, Gen Zhang, Jianjing Cui, and Jun Long. A survey of clustering with deep learning: From the perspective of network architecture. *IEEE Access*, 6:39501–39514, 2018.

[28] Ari Pakman, Yueqi Wang, Catalin Mitelut, Jinyung Lee, and Liam Paninski. Neural clustering processes. *arXiv: Machine Learning*, 2019.

[29] Jeong Joon Park, Peter Florence, Julian Straub, Richard Newcombe, and Steven Lovegrove. Deepsdf: Learning continuous signed distance functions for shape representation. In *Proceedings of the IEEE Conference on Computer Vision and Pattern Recognition*, pages 165–174, 2019.

[30] Adam Santoro, Ryan Faulkner, David Raposo, Jack Rae, Mike Chrzanowski, Theophane Weber, Daan Wierstra, Oriol Vinyals, Razvan Pascanu, and Timothy Lillicrap. Relational recurrent neural networks. In *Advances in neural information processing systems*, pages 7299–7310, 2018.

[31] ShiJie Sun, Naveed Akhtar, HuanSheng Song, Ajmal Mian, and Mubarak Shah. Deep affinity network for multiple object tracking. In *TPAMI*, June 2019.

[32] Aviv Tamar, Sergey Levine, Pieter Abbeel, Yi Wu, and Garrett Thomas. Value iteration networks. *ArXiv*, abs/1602.02867, 2016.

[33] Greg Welch and Gary Bishop. An introduction to the kalman filter. 2006.

[34] Fei Xia, William B Shen, Chengshu Li, Priya Kasimbeg, Micael Edmond Tchapmi, Alexander Toshev, Roberto Martín-Martín, and Silvio Savarese. Interactive gibson benchmark: A benchmark for interactive navigation in cluttered environments. *IEEE Robotics and Automation Letters*, 5(2):713–720, 2020.

[35] Yu Xiang, Alexandre Alahi, and Silvio Savarese. Learning to track: Online multi-object tracking by decision making. In *Proceedings of the IEEE international conference on computer vision*, pages 4705–4713, 2015.

VII. APPENDIX

In the appendix, we first provide additional experimental analysis of our approach in Section VIII. Next we provide an analysis of our sparsity loss in Section IX. Finally we provide experimental details for each setting of our approach in Section X.

VIII. ADDITIONAL EXPERIMENTAL ANALYSIS

We provide additional experimental analysis of OBM-Net. First we show that OBM-Net is able to discover more objects than the number it was trained on. Next, we provide qualitative illustrations of OBM-Net fitting 2D clusters. We then provide an analysis of OBM-Net on a large number of clusters and finally provide full quantitative results on all clustering settings.

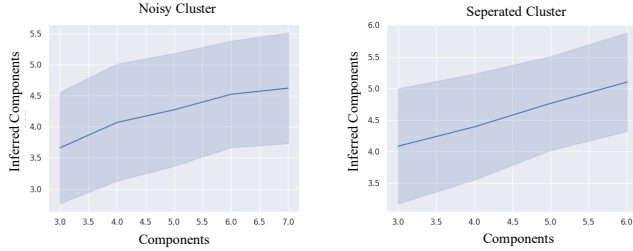


Fig. 6: Plots of inferred number of components using a confidence threshold in OBM-Net compared to the ground truth number of clusters (OBM-Net is trained on only 3 clusters). We consider two scenarios, a noisy scenario where cluster centers are randomly drawn from -1 to 1 (left) and a scenario where all added cluster components are well separated from each other (right). OBM-Net is able to infer more clusters in both scenarios, with better performance when cluster centers are more distinct from each other.

A. Discovery of Objects

In contrast to other algorithms, OBM-Net learns to predict both a set of object properties y_k of objects and a set of confidences c_k for each object. This corresponds to the task of both predicting the number of objects in a set of observations, as well as the associated object properties. We evaluate the

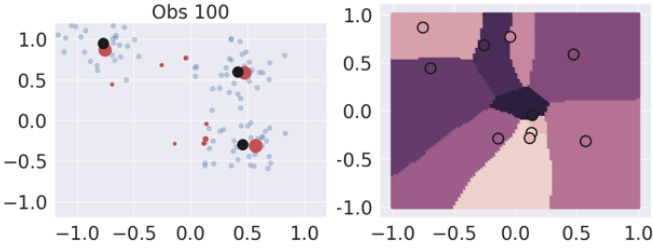


Fig. 7: Plot of decoded values of slots (in red) with confidence shown by the size of dot (left), and what slot each input assigns the highest attention towards (right) (each slot is colored differently, with assigned inputs colored in the same way). Note alignment of regions on the right with the decoded value of a slot on the left.

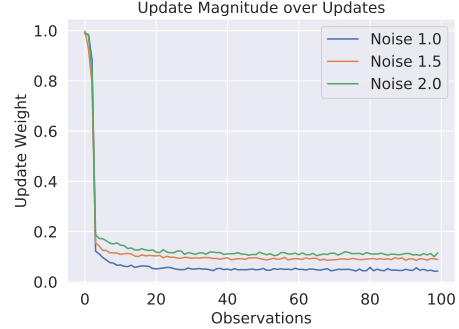


Fig. 8: Plots of the magnitude of relevance weights with increased observation number on different distributions with higher standard deviation (noise).

ability to regress object number in OBM-Net in scenarios where the number of objects is different than that of training. We evaluate on the Normal distribution with a variable number of component distributions, and measure inferred components through a threshold confidence. OBM-Net is trained on a dataset with 3 underlying components.

We find in Figure 6 that OBM-Net is able to infer the presence of more component distributions (as they vary from 3 to 6), with improved performance when cluster centers are sharply separated (right figure of Figure 6).

B. Qualitative Visualizations

We provide an illustration of our results on the *Normal* clustering task in Figure 9. We plot the decoded values of hypothesis slots in red, with size scaled according to confidence, and ground-truth cluster locations in black. OBM-Net is able to selectively refine slot clusters to be close to ground truth cluster locations even with much longer observation sequences than it was trained on.

We find that each component learned by OBM-Net is interpretable. We visualize the attention weights of each hypothesis slot in Figure 7 and find that each hypothesis slot learns to attend to a local region next to the value it decodes to. We further visualize a plot of relevance weights in Figure 8 across an increasing number of observations over different levels of noise in each distribution. We find that as we see more observations, the relevance weight of new observations decreases over time, indicating that OBM-Net learns to pay the most attention towards the first set of observations it sees. In addition, we find that in distributions with higher variance, the relevance weight decreases more slowly, as later observations are now more informative in determining cluster centers.

C. Performance Using More Clusters

We measure the performance OBM-Net in the presence of a large number of clusters and slots. We consider the *Normal* distribution setting, where input observations are generated by a total of 30 difference clusters. We train OBM-Net with 50 observations, and measure performance at inferring cluster centers with either 50 or 100 observations. We report

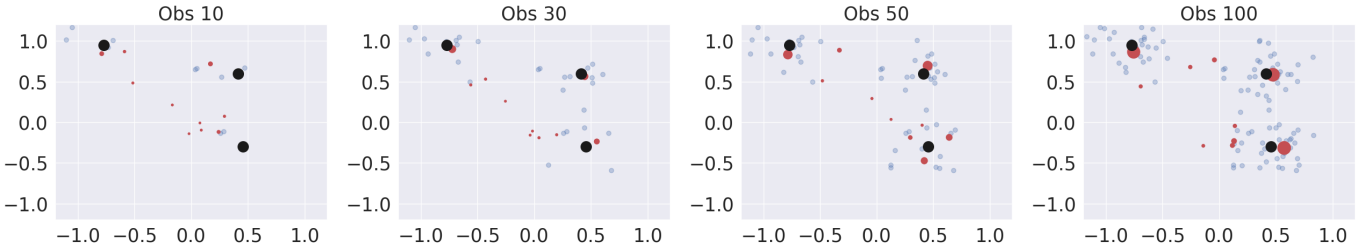


Fig. 9: Illustration of the clustering process. Decoded value of hypothesis (with size corresponding to confidence) shown in red, with ground truth clusters in black. Observations are shown in blue.

Model	Online	Observations			
		50	65	80	100
OBM-Net	+	0.158 (0.001)	0.154 (0.001)	0.151 (0.001)	0.147 (0.001)
VQ	+	0.162 (0.001)	0.157 (0.001)	0.153 (0.001)	0.148 (0.001)
K-means++	-	0.155 (0.001)	0.151 (0.001)	0.148 (0.001)	0.146 (0.001)
GMM	-	0.156 (0.001)	0.151 (0.001)	0.149 (0.001)	0.147 (0.001)

TABLE X: Comparison of performance on Normal distribution. We use 30 components, and train models with 50 observations. We report standard error in parentheses. Each cluster observation and center is drawn between -1 and 1, with reported error as the L2 distance between predicted and ground truth means.

performance in Table X and find that OBM-Net approach obtains good performance in this setting, out-performing both online and offline baselines.

D. Full Quantitative Results

We report full performance of each different model across different distributions in Table XI. We find that OBM-Net is able to obtain better performance with increased number of observations across different distributions. In addition OBM-Net outperforms neural network baselines when evaluated on 30 observations across distributions except for rotation. For rotation we find that when training with 10,000 different distributions, OBM-Net exhibits better performance of 0.555 compared to Set Transformer Online performance of 0.647 and LSTM performance of 0.727.

IX. SPARSITY LOSS

In this section, we show that $\mathcal{L}_{\text{sparse}}(\mathbf{c})$ encourage confidences \mathbf{c} to be sparse. Recall that

$$\mathcal{L}_{\text{sparse}}(\mathbf{c}) = -\log\|\mathbf{c}\| . \quad (1)$$

where $\|\mathbf{c}\|$ is the L2 norm which is convex. Recall that \mathbf{c} , the confidence vector, defines a polyhedron, since it is the set of points that are non-negative, and whose elements sum up to one. The maximum of a convex function over a polyhedron must occur at the vertices, which correspond to an assignment of 1 to a single c_i and 0s to every other value of \mathbf{c} . Next we consider the minimum of $\|\mathbf{c}\|$ given that its elements sum up to one. This is equivalent to finding the stationary points of the Legrangian

$$\sum_i c_i^2 + \lambda(\sum_i c_i - 1) \quad (2)$$

By taking the gradient of the above expression, we find that the stationary value corresponds to each c_i being equal. Since the function is convex, this corresponds to the minimum of $\|\mathbf{c}\|$. Thus $\mathcal{L}_{\text{sparse}}(\mathbf{c})$ is maximized when each individual confidence is equal.

X. EXPERIMENTAL DETAILS

In this section, we prevent details of our experimental approach. We first discuss the underlying parameters utilized in each of our training settings. Next, we provide the model architectures used in experiments. Finally, we provide details on the baselines we compare with.

A. Dataset Details

We first provide detailed experimental settings for each Gaussian distribution below. Gaussian centers are drawn uniformly from -1 to 1.

- 1) *Normal*: Each 2D Gaussian has standard deviation 0.2. The normal setting is illustrated in Figure 10.
- 2) *Mixed*: Each distribution is a 2D Gaussian, with fixed identical variance across each individual dimension, but with the standard deviation of each distribution drawn from a uniform distribution from (0.04, 0.4).
- 3) *Elongated*: Each distribution is a 2D Gaussian, where the standard deviation along each dimension is drawn from a uniform distribution from (0.04, 0.4), but fixed across distributions.
- 4) *Angular*: Each distribution is a 2D Gaussian with identical standard deviation across dimension and distribution, but points above π are wrapped around to $-\pi$ and points below $-\pi$ wrapped to π . Gaussian means are selected between $(-\pi, -2\pi/3)$ and between $(2\pi/3, \pi)$. The standard deviation of distributions is $0.3 * \pi$.
- 5) *Noise*: Each distribution has 2 dimensions parameterized by Gaussian distributions with standard deviation 0.5, but with the values of the remaining 30 dimensions drawn from a uniform distribution from $(-1, 1)$.

For dynamics settings, we implement our dataset using the StoneSoup library*. We initialize the location of each cluster from a Gaussian distribution with standard deviation 1.5 and initialize velocity in each directory from a Gaussian distribution with standard deviation of 0.02. At each timestep, Gaussian noise is added to velocities with magnitude 1e-4. We show

*<https://stonesoup.readthedocs.io/en/v0.1b3/stonesoup.html>

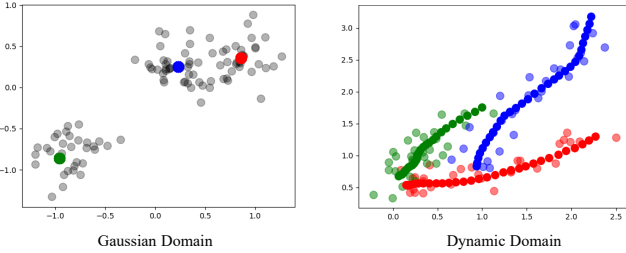


Fig. 10: Visualizations of the Normal Gaussian and Dynamic domains. Observations are transparent while ground truth states are bolded.

example tracks in Figure 10. Our JPDA implementation is also from the StoneSoup library.

For robotics domains, we implement our embodied house environment Pybullet, and construct a house with x and y axis between -1 and 1. We utilize furniture assets from [34]. Each table has size 0.15 by 0.1.

B. Model/Baseline Architectures

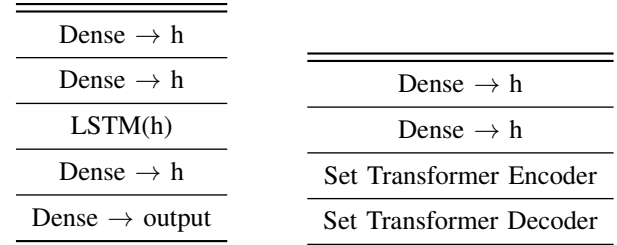
We provide the overall architecture details for the LSTM in Figure 11a, for the set-transformer in Figure 11b and OBM-Net in Figure 12a. For image experiments, we provide the architecture of the encoder in Figure 13a and decoder in Figure 13b. Both LSTM, OBM-Net, and autoencoding baselines use the same image encoder and decoder. For robotics experiments, we provide the architecture of the shape decoder in Figure 12b.

In OBM-Net memory, the function $\text{update}(s_k, n_k, e)$ is implemented by applying a 2 layer MLP with hidden units h which concatenates the vectors s_k, n_k, e as input and outputs a new state u_k of dimension h . The value n_k is encoded using the function $\frac{1}{1+n_k}$, to normalize the range of input to be between 0 and 1. The function $\text{attend}(s_k, n_k, e)$ is implemented in an analogous way to update, using a 2 layer MLP that outputs a single real value for each hypothesis slot.

For the function $\text{relevance}(s_k, n_k, e)$, we apply NN_1 per hypothesis slot, which is implemented as a 2 layer MLP with hidden units h that outputs a intermediate state of dimension h . (s_k, n_k, e) are fed into NN_1 in an analogous manner to update. NN_2 is applied to average of the intermediate representations of each hypothesis slot and is also implemented as a 2 layer MLP with hidden unit size h , followed by a sigmoid activation. We use the ReLU activation for all MLPs. NN_3 is represented is GRU, which operates on the previous slot value.

C. Baseline Details

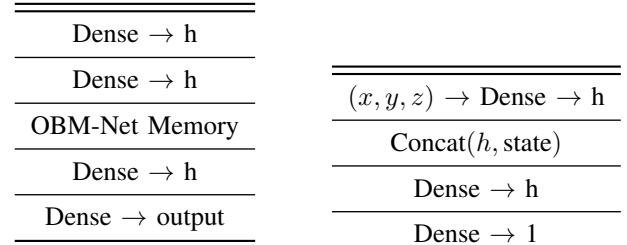
All baseline models are trained using prediction slots equal to the ground truth of components. To modify the set transformer to act in an online manner, we follow the approach in [30] and we apply the Set Transformer sequentially on the concatenation of an input observation with hypothesis slots. Hypothesis slots are updated based off the new values of the slots after applying self-attention (Set Transformer Encoder). We use the Chamfer loss to train baseline models, with confidence set to 1.



(a) The model architecture of the LSTM baseline. The hidden dimension h used is 96 for synthetic Gaussian distributions and 128 for Image datasets. For image experiments, the first 2 and last 2 fully connected layers are replaced with image encoders and decoders.

(b) The model architecture of the Set Transformer baseline. The hidden dimension h is 48 for the synthetic Gaussian distributions. We use the encoder and decoder defined in [19] with 4 heads and hidden dimension h .

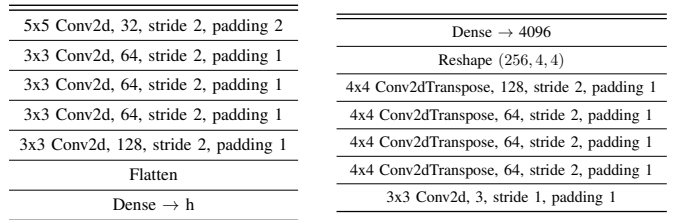
Fig. 11: Architecture of baseline models.



(a) The model architecture of OBM-Net. The hidden dimension h is 64 is for synthetic Gaussian distributions and 128 for the image/robotics experiments. For image experiments, the first and last 2 linear layers are replaced with convolutional encoders and decoders.

(b) The shape decoder of OBM-Net used in the robotics experiments. The shape decoder takes as input a voxel coordinate as well as a slot value and predicts a occupancy for the voxel.

Fig. 12: Architecture of OBM-Net and the shape decoder.



(a) The model architecture of the convolutional encoder for image experiments.

(b) The model architecture of the convolutional decoder for image experiments.

Fig. 13: The model architecture of the convolutional encoder and decoder for image experiments.

Type	Model	Online	Observations			
			10	30	50	100
Normal	OBM-Net	+	0.235 (0.001)	0.162 (0.001)	0.146 (0.001)	0.128 (0.001)
	Set Transformer	+	0.390 (0.002)	0.388 (0.002)	0.388 (0.002)	0.389 (0.001)
	LSTM	+	0.288 (0.001)	0.260 (0.001)	0.269 (0.001)	0.288 (0.001)
	VQ	+	0.246 (0.001)	0.172 (0.001)	0.147 (0.001)	0.122 (0.001)
	Set Transformer	+	0.295 (0.003)	0.261 (0.001)	0.253 (0.001)	0.247 (0.001)
	K-means++	-	0.183 (0.002)	0.107 (0.001)	0.086 (0.001)	0.066 (0.001)
	GMM	-	0.189 (0.002)	0.118 (0.001)	0.087 (0.001)	0.067 (0.001)
Mixed	OBM-Net	+	0.255 (0.002)	0.184 (0.001)	0.164 (0.001)	0.147 (0.001)
	LSTM	+	0.306 (0.002)	0.274 (0.001)	0.284 (0.001)	0.290 (0.001)
	Set Transformer	+	0.415 (0.002)	0.405 (0.001)	0.407 (0.001)	0.408 (0.001)
	VQ	+	0.262 (0.002)	0.192 (0.001)	0.169 (0.001)	0.145 (0.001)
	Set Transformer	-	0.309 (0.002)	0.274 (0.001)	0.266 (0.001)	0.261 (0.001)
	K-means++	-	0.206 (0.003)	0.135 (0.001)	0.105 (0.001)	0.088 (0.001)
	GMM	-	0.212 (0.003)	0.136 (0.001)	0.105 (0.001)	0.079 (0.001)
Elongated	OBM-Net	+	0.258 (0.002)	0.192 (0.001)	0.173 (0.001)	0.161 (0.001)
	LSTM	+	0.314 (0.003)	0.274 (0.002)	0.288 (0.001)	0.300 (0.001)
	Set Transformer	+	0.394 (0.003)	0.391 (0.003)	0.394 (0.003)	0.394 (0.003)
	VQ	+	0.265 (0.003)	0.194 (0.002)	0.172 (0.001)	0.149 (0.001)
	Set Transformer	-	0.309 (0.002)	0.244 (0.002)	0.240 (0.001)	0.232 (0.001)
	K-means++	-	0.213 (0.002)	0.139 (0.001)	0.113 (0.001)	0.092 (0.001)
	GMM	-	0.214 (0.002)	0.141 (0.001)	0.112 (0.001)	0.086 (0.001)
Rotation	OBM-Net	+	0.892 (0.001)	0.794 (0.001)	0.749 (0.002)	0.736 (0.001)
	LSTM	+	0.799 (0.003)	0.796 (0.002)	0.795 (0.002)	0.794 (0.002)
	Set Transformer	+	0.793 (0.003)	0.794 (0.002)	0.782 (0.002)	0.782 (0.002)
	VQ	+	0.956 (0.003)	1.00 (0.003)	1.00 (0.003)	0.984 (0.003)
	Set Transformer	-	0.815 (0.003)	0.784 (0.002)	0.779 (0.002)	0.772 (0.002)
	K-means++	-	0.827 (0.004)	0.834 (0.003)	0.823 (0.002)	0.802 (0.001)
	GMM	-	0.842 (0.004)	0.875 (0.001)	0.867 (0.003)	0.848 (0.002)
Noise	OBM-Net	+	0.375 (0.001)	0.343 (0.001)	0.338 (0.001)	0.334 (0.001)
	LSTM	+	0.419 (0.001)	0.406 (0.001)	0.405 (0.001)	0.407 (0.001)
	Set Transformer	+	0.434 (0.001)	0.424 (0.001)	0.425 (0.001)	0.424 (0.001)
	VQ	+	1.479 (0.002)	0.948 (0.002)	0.826 (0.001)	0.720 (0.001)
	Set Transformer	-	0.436 (0.001)	0.407 (0.002)	0.398 (0.001)	0.394 (0.001)
	K-means++	-	1.836 (0.002)	1.271 (0.002)	1.091 (0.002)	0.913 (0.002)
	GMM	-	1.731 (0.002)	1.215 (0.002)	1.056 (0.002)	0.856 (0.002)

TABLE XI: Comparison of performance under different settings after training on different distribution for a thousand iterations. We use a total of 3 components, and train models with 30 observations. We report standard error in parentheses.